UNIVERSITY *of* York

This is a repository copy of *Selected Ion Flow Tube – Mass Spectrometry (SIFT-MS) study of the reactions of H3O+, NO+ and O2+ with a range of oxygenated volatile organic carbons (OVOCs)*.

White Rose Research Online URL for this paper:
https://eprints.whiterose.ac.uk/189756/

Version: Published Version

White Rose
university consortium
Universities of Leeds, Sheffield & York

eprints@whiterose.ac.uk
https://eprints.whiterose.ac.uk/
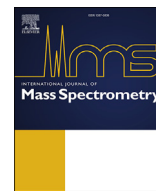
Selected Ion Flow Tube − Mass Spectrometry (SIFT-MS) study of the reactions of H_3O^+, NO^+ and O_2^+ with a range of oxygenated volatile organic carbons (OVOCs)

Ieuan J. Roberts [a,*], Lucy J. Carpenter [a], Marvin D. Shaw [a], Vaughan S. Langford [b]

[a] *Wolfson Atmospheric Chemistry Laboratories, University of York, York, YO10 5DQ, United Kingdom*
[b] *Syft Technologies Limited, 68 Saint Asaph Street, Christchurch, 8011, New Zealand*

ARTICLE INFO

ABSTRACT

Selected Ion Flow Tube-Mass Spectrometry (SIFT-MS) uses soft chemical ionisation, typically by H_3O^+, NO^+ and O_2^+, to analyse trace gases in real time at mixing ratios down to low parts per trillion by volume (pptv) and has recently been demonstrated as an effective method for monitoring volatile organic compounds (VOCs) in the atmosphere. SIFT-MS analysis requires accurate rate coefficient and product ion branching ratio data to allow for accurate mixing ratio calculations without the need for calibration standards. Most rate constant data have been measured using helium as the carrier gas. Here we report rate constants of a number of oxygenated volatile organic compounds (OVOCs) alongside benzene for H_3O^+, NO^+ and O_2^+ reagent ions in nitrogen carrier gas, using a permeation tube calibration source and a certified gas standard to introduce known concentrations into the SIFT-MS. This includes the first reported literature rate constant for nonanal using SIFT-MS. We found that the rate constants for most compounds measured in nitrogen carrier gas were similar to those measured in helium. However, the NO^+ rate constants for ketones measured in nitrogen were 1.2−5 times lower than those measured in helium. We observe higher fragmentation due to changes made to the lens voltages of the instrument in order to tune for higher sensitivity, altering the reagent ion energies. We also show the impact of increasing the flow tube temperature and voltage on the sensitivity and ionisation of benzene, butanone and butanal under both dry and humid conditions. Some of the SIFT-MS compound library entries are data from historic SIFT-MS instruments that lacked a heated flow tube, and therefore suffered from higher water clustering than current commercial SIFT-MS models. We show that a higher flow tube temperature reduces the amount of water adduct formation thereby simplifying compound concentration determination. These results demonstrate the need to ensure that the library data used are acquired under the same conditions as the experiment being performed.

© 2022 The Authors. Published by Elsevier B.V. This is an open access article under the CC BY license (http://creativecommons.org/licenses/by/4.0/).

1. Introduction

1.1. OVOCs in the atmosphere

OVOCs are air pollutants which can impact the atmospheric oxidative capacity and, tropospheric ozone, affecting human health and Earth's climate. OVOCs have a range of sources, from primary biogenic [1−3] and anthropogenic [3,4] to secondary atmospheric sources [3,5,6] resulting from photochemical processing of primary hydrocarbon emissions. OVOCs can impact human health through both direct exposure and secondary chemistry [7−10]. OVOCs can be an important sink of hydroxyl (OH) radicals, reducing the oxidative capacity and impacting the O_3 mixing ratio [11−15]. OVOCs like formic acid, and other low volatility OVOCs, can contribute to both new particle growth [16] and the formation of secondary organic aerosol [17].

The most abundant OVOCs in the marine atmosphere are formaldehyde (~70 pptv - 20 ppbv) [18−27], acetaldehyde (~60 pptv - 8 ppbv) [11,18,20−22,24−32], acetone (~200 pptv - 11 ppbv) [11,18,21−23,25,26,28−35] and methanol (300 pptv − 1.6 ppbv) [11,29−31,34]. Global models underestimate the concentration of many OVOCs in the lower marine atmosphere, including acetaldehyde [36], glyoxal [37] and methanol [38]. A recent study found a

correlation between missing OH reactivity in the marine boundary layer with formaldehyde, dimethyl sulfide, butanal and sea surface temperature which suggests the presence of either unmeasured or unknown OVOC emitted from the ocean [39]. The sea surface microlayer (SML), a 10−1000 μm ubiquitous layer across the ocean surface concentrated in surfactants, has been shown to be a potentially rich source of OVOCs to the ocean atmosphere [40−43]. A number of studies have been performed on compounds that are used as proxies, to represent the complex mixture of the SML, such as oleic acid and nonanal, to analyse the products produced formed via ozonolysis and photochemistry. These studies report the production of a range of OVOC compound classes including aldehydes, ketones, acids and dicarbonyls, both saturated and unsaturated [41,44−48]. This shows that OVOCs like aldehydes and organic acids are major products of ozonolysis and photochemical reactions expected to occur at the ocean surface and points to a need to quantify the emissions and abundance of atmospheric OVOCs beyond the simple C1−C3 compounds commonly studied.

1.2. SIFT-MS

SIFT-MS is a soft chemical ionisation mass spectrometry method that can quickly switch between reagent ions to provide both a wide range of potential target compounds and high selectivity for compound discrimination. It enables real time detection and quantification of complex mixtures such as ambient air that would be much more challenging using conventional electron ionisation mass spectrometry. To date, three studies have reported field measurements of atmospheric VOCs by SIFT-MS. Prince et al. [49] measured toluene, 1,3-buitadiene, benzene, ethanol and ethene in ambient air in suburban Christchurch, New Zealand, finding mixing ratios from high ppt to low ppb levels, and were able to suggest common sources of certain compounds due to the consistent real time sampling. Wagner et al. [50] measured a suite of VOCs from a mobile van on a road circuit through York, UK, allowing for highly resolved temporal and spatial measurements and identifying hotspots of specific compounds. Hien et al. [51] measured 22 VOCs in Hanoi, Vietnam, in March 2019 demonstrating that the VOC mix was dominated by OVOCs (43%) and alkanes (14%). These studies illustrate the utility of a real time system like SIFT-MS for performing atmospheric measurements.

In SIFT-MS, a microwave ion-source fed by humid air is used to generate a mixture of positive ions [52]. These include the primary reagent ions H_3O^+, NO^+ and O_2^+ which are individually m/z selected by an upstream quadrupole (Fig. 1) to produce a stream of specific reagent ions. These ions are injected into an inert carrier gas (helium or nitrogen) through a Venturi orifice. The reagent ion stream travels through a heated flow tube for a set distance before being introduced to the sample flow which is injected into the flow tube perpendicular to the reagent ion flow. Reactions occur through the remainder of the flow tube (which can be of various geometries, here it bends 90°). Note that reaction effectively stops at the end of the flow tube due to the pressure drop into either the ion guide (if present) or the downstream quadrupole The downstream quadrupole can be set to either scan through an m/z range or transmit specific m/z ions which correspond to the product ions of the analyte. These individual m/z ions are then detected by a particle multiplier and pulse counting system. A simplified schematic of the instrument is shown in Fig. 1. The instrument has been described in detail by Prince et al. [49].

1.3. SIFT-MS studies of benzene and OVOCs

Ionisation rate constants of a range of compounds reacting with different reagent ions have been measured using SIFT-MS. Many of these studies were performed by Smith and Spanel [53] in the late 90s and are still used. Smith and Spanel [54] utilised the fact that proton transfer, when exothermic, generally proceeds at or very close to the collision limited rate constant, k_C. This allowed them to use the calculated k_C as a proxy for the H_3O^+ rate constant. Experimental NO^+ and O_2^+ rate constants were typically derived by introducing a known concentration of the target analyte into a plastic bag, sampling this into the instrument and then observing the decay curves of all three reagent ions simultaneously as a function of flow rate. The gradients of the NO^+ and O_2^+ reagent ions were then used to calculate the rate constants relative to the H_3O^+ rate constant. These experiments were performed on precommercial research instruments.

Recent work by Spanel et al. [55] utilised the vapour headspace of a bottle mixture of alcohols in water to measure the impacts of humidity on the product ion formation of the system. This was performed on a Profile 3 SIFT-MS (Profile 3, Instrument Science Limited, Crewe, UK) using helium as a carrier gas at a temperature of 27 °C and a pressure of 1 Torr. This temperature is much lower than the factory pre-set tube temperature in the Voice200*ultra* (Voice200*ultra*, Syft Technologies, Christchurch, NZ) produced by Syft Technologies of 120 °C. The Spanel et al. [55] study did not attempt to measure rate constants and was only focused on determining the impact of humidity on the product ions of the reaction. The study found major impacts from humidity at this low flow tube temperature, with methanol and propanol exhibiting double clustering, forming $MH^+(H_2O)_2$ ions. At an absolute sample humidity of 3.5% the double clustering ion accounted for 50% of the methanol and 40% of the propanol total ion counts, with the singular water cluster accounting for 30% of the methanol and 10% of the propanol total ion counts. This means that the dry product ion count for methanol was only 20% at 3.5% sample humidity.

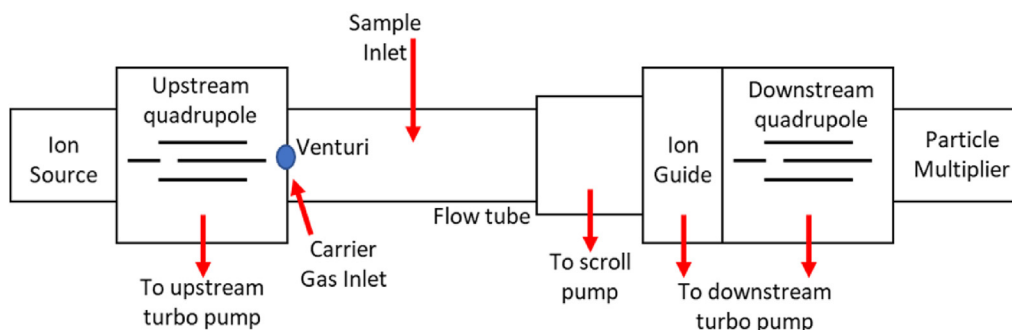It is important to note that most rate constant data have been

Fig. 1. Schematic of the Voice200ultra model of the SIFT-MS instrument produced by Syft Technologies Ltd.

measured using helium as the carrier gas. As global helium supplies become increasingly scarce, more users will start moving towards nitrogen as a cheap and renewable alternative carrier gas. The depleting supply of helium is compounded by leaks and fires that have caused recent unplanned shutdowns of helium processing plants [56,57]. The recent war in Ukraine has also increased concern on the supply of helium from Russia [56,57]. This presents problems for some applications of SIFT-MS as the library of compounds measured in nitrogen is much smaller. One issue with nitrogen as a carrier gas compared to helium is that the energy in the system is higher, particularly when energetic collisions are encouraged by voltage gradients during injection or extraction, meaning that the H_3O^+ ions can collide with N_2 molecules to form fragment ions like $H_2O^{+\bullet}$ and OH^+ which can potentially alter the ion chemistry in the instrument [58]. Also, at a pressure of 0.5 mbar and room temperature, the N_2 carrier gas readily forms adducts such as $H_3O^+N_2$ which is a catalyst to water clustering [58]. This can be mitigated by increasing the temperature of the carrier gas [59]. Nitrogen also has a higher efficiency for collisional cooling than helium [60], which means adduct product ions are favoured in nitrogen compared to helium. The importance of developing the database for measurements in N_2 carrier gas was recently emphasized by Smith et al. [58].

In this work, the rate constants, product ions and branching ratios of the reaction of SIFT-MS reagent ions with a range of OVOC compounds were measured with nitrogen as the carrier gas. The measurement of benzene was used as a standard to evaluate the accuracy of the data as benzene is a well characterised compound in SIFT-MS. To minimize water clustering, our measurements are made at a flow tube temperature of 140 °C, much higher than the 27 °C temperatures of previous studies [53,54,61], [−] [64] and 20 °C higher than the standard operating temperature of the Voice200*ultra*.

2. . Methods and experimental

2.1. Calibration and permeation tube methodology

Permeation tubes are commonly used to deliver stable concentrations of compounds for calibration [65,66]. Permeation tubes are useful for calibration of trace gases as many exist in the liquid phase under standard conditions. In this work, permeation tubes were made from ¼″ PTFE tubing with an internal diameter of 5.8 mm (wall thickness of 0.275 mm) with either brass or stainless-steel Swagelok fittings as caps. An 8 cm length of tubing was used, when including the Swagelok fittings this gave an approximately 5 cm permeation window.

All chemicals were obtained from Sigma-Aldrich, except for butanal which was purchased from Merck, and had the following purities: benzene (≥99%), butanal (99%), 2-butenal (≥99.5%), 2-butanone (≥99.9%), hexanal (98%), 2-hexenal (98%), 2-octanone (98%), 2-pentanone (≥98%), 1-propanol (99.7%) and nonanal (99%). These compounds were chosen as they have been identified as potentially significant atmospheric emissions from the surface of seawater [41,67−70].

A certified gas standard (National Physics Laboratory, NPL) containing a mixture of 14 gases was also used for verification of some measurements, containing; methanol (1.03 ± 0.10 ppm), ethanol (0.99 ± 0.05 ppm), acetonitrile (1.02 ± 0.03 ppm), acetone (1.01 ± 0.05 ppm), isoprene (1.01 ± 0.05 ppm), butenone (1.03 ± 0.05 ppm), 2-butanone (1.01 ± 0.05 ppm), benzene (1.03 ± 0.03 ppm), toluene (1.04 ± 0.03 ppm), *m*-xylene (1.02 ± 0.05 ppm), 1,2,4-trimethylbenzene (1.02 ± 0.03 ppm), 1,3-butadiene (1.04 ± 0.03 ppm), n-octane (1.02 ± 0.05 ppm), n-nonane (1.01 ± 0.10 ppm), n-decane (1.01 ± 0.10 ppm) and n-dodecane

(1.00 ppm).

Fig. 2 shows the setup that was used for all SIFT-MS experiments. The permeation ovens temperatures were individually controlled by temperature controllers (6100+, West Control Solutions, Gurnee, IL, USA). The nitrogen gas is generated by a Nitrogen Generator (Infinity NM32L, Peak Scientific, Inchinnan, UK). When measuring from the calibration gas cylinder (NPL) the cylinder was attached at the same T-junction the permeation oven outlet attaches to during normal measurement. The permeation oven was unattached during these calibration cylinder measurements.

For humid scans the flow setup had to be modified to allow the diluent to flow through a dew-point generator (DG3, Michell Instruments, Ely, UK). This was placed in between the mass flow controller F2 and the t-piece seen in Fig. 4. This allowed a flow with a relative humidity of up to 100% to be generated, which was then diluted by the introduction of the permeation flow. The flow rates through F2 and the humidity generator were variable, between 0.05 and 1.00 sccm (standard cubic centimetres), allowing for the humidity to be altered. Humid scans were performed identically to a full mass scan, only with a humid diluent flow rather than a dry diluent flow. The scans were performed over a range of diluent flows.

Each permeation tube was weighed approximately every fortnight, with each weighing repeated 3 times to ensure a stable value. The permeation rate of each compound was calculated as the ratio of the gradient of the mass loss over time divided by the molecular mass of the given compound. This was then converted directly into a concentration by choosing a standard exposure time and the mixing ratio calculated by dividing this concentration by the moles of carrier gas passed through the permeation oven in the given exposure time.

2.2. SIFT-MS operating conditions

The Voice200*ultra* was operated with two major changes from the standard operating conditions. Firstly, the flow tube temperature was 20 °C higher than operationally recommended by the manufacturer and over 100 °C higher than the flow tube temperature used in older literature by Smith and Spanel.

Secondly, the lens voltages in our SIFT-MS have been tuned to improve the sensitivity of the instrument. These same lens voltages were used by Wagner et al. [50] in their study. The major change from the lens voltages we have adopted for atmospheric measurements [50], compared to those of a standard Voice200*ultra* is an increase of the upstream FT voltage from 25 V to 50 V. The lens voltages were increased in order to increase transmission of ions through the flow tube. However, this change, and other minor changes to other lenses, affects the ion energetics of the instrument.

Experiments were performed at a range of flow tube temperatures (38 °C, 120 °C and 140 °C) and flow tube voltages (25 V and 50 V) under both dry and humid conditions to ascertain the impacts on both sensitivity and product ion chemistry. Due to the curve of the flow tube in the Syft200ultra the flow tube voltage could not be reduced to 0 V as used in other SIFT-MS instruments as a small flow tube voltage is required to guide the reagent and product ions through the flow tube.

We tested benzene, butanal and butanone over the six combinations of flow tube temperatures and voltages.

All experiments were performed with a nitrogen carrier gas flow rate of 172 ± 4 sccm with a sample inlet flow rate of 25 sccm. This meant the sample flow was always 14−15% of the total flow through the instrument. For the production of reagent ions we found that, under dry conditions, the increase of temperature gradually reduced the overall H_3O^+ reagent ion count by reducing
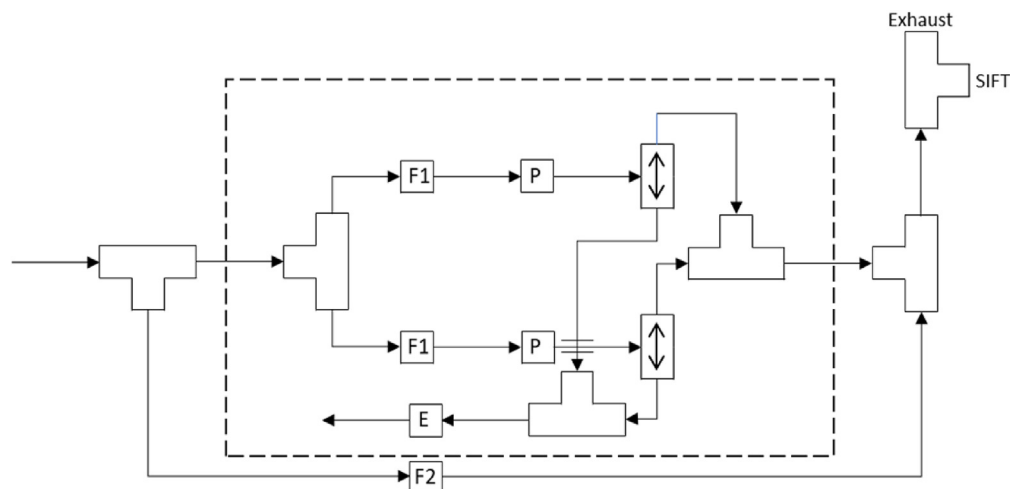
Fig. 2. The permeation tube calibration system. F1 are 100 sccm mass flow controllers (FC-280SA, Tylan, and 1179A, MKS Instruments, Andover, MA, USA), F2 is a 0−10 slpm (standard litres per minute) mass flow controller (10-SLPM-D, Alicat Scientific, Tucson, AZ, USA) which controls diluent flow, P are permeation ovens, E is an exhaust filter and the dashed box shows the permeation oven casing.
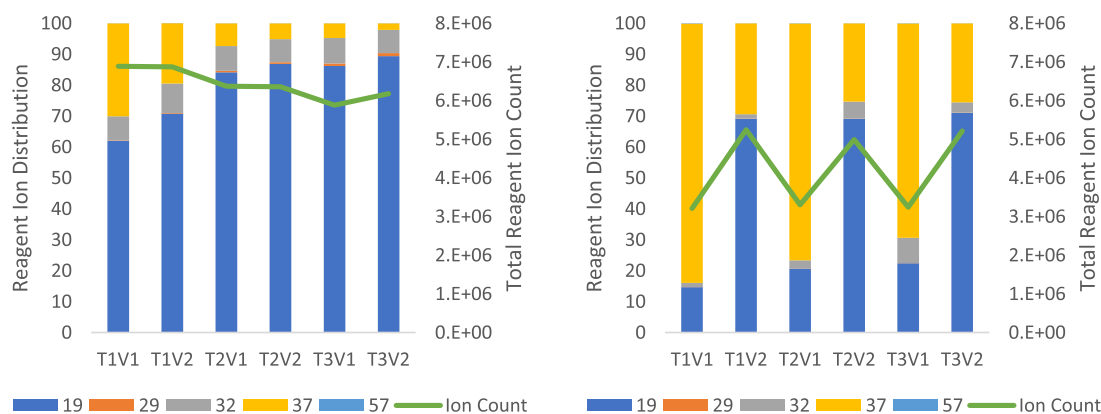
Fig. 3. H_3O^+ reagent ion counts and distribution under dry (left) and humid conditions (right). The temperatures and voltages are denoted by the column labels where T1 = 38 °C, T2 = 120 °C, T3 = 140 °C, V1 = 25 V and V2 = 50 V.

the $H_3O^+.H_2O$ ion count with no large impact on the reagent ion counts for NO^+ or O_2^+. The increase in voltage caused an increase in the proportion of the H_3O^+ reagent ion in the H_3O^+ channel without reducing the overall reagent ion count but did reduce the reagent ion count in the NO^+ channel by 15% and in the O_2^+ channel by 10%.

Under humid conditions (sample flow of roughly 100% relative humidity) the increase in temperature had little impact on the total ion count in the H_3O^+ and NO^+ channel and increased the ion count of the O_2^+ channel. The increase in temperature slightly increased the proportion of H_3O^+ to $H_3O^+.H_2O$ in the H_3O^+ channel (Fig. 3) and the proportion of the O_2^+ reagent ion in the O_2^+ channel, see Fig. S2 (*'S' referring to the supplementary information*). Increasing the temperature did introduce slight fragmentation in the NO^+ channel (Fig. S1), but no more than under dry conditions. Increasing the flow tube voltage caused a large increase in the H_3O^+ channel ion count, both increasing the total and percentage of the H_3O^+ reagent ion in the H_3O^+ channel as shown in Fig. 3. The increased voltage also caused a slight reduction in the NO^+ ion count and a large increase in the O_2^+ reagent ion count in the O_2^+ channel, associated with an increase of H_3O^+ reagent ion in the O_2^+ channel.

Under dry conditions the increase in temperature caused a consistent decrease in sensitivity. The increase of the flow tube

voltage in dry conditions caused little change in the sensitivity of benzene (Fig. S3) and butanal (Fig. S6) but a large decrease in the sensitivity of butanone (Fig. S10), attributed to a large drop in the NO^+ sensitivity. This is likely due to increased energy being unfavourable to adduct formation reactions, the major product ion of ketones with NO^+. Under humid conditions increasing the temperature decreased the sensitivity of benzene (Fig. S3) but led to an increase in sensitivity of both butanal (Fig. S6) and butanone (Fig. S10). Increasing the voltage caused no real change in the sensitivity of benzene but increased the sensitivity of butanal and again decreased the sensitivity of butanone. The decreased butanone sensitivity is again driven by a loss of NO^+ sensitivity but, like with the butanal, is accompanied by an increased H_3O^+ sensitivity.

For benzene, increasing the temperature and voltage had no large impact on the H_3O^+ product ion distribution (Fig. S4) but greatly reduced the NO^+ adduct formation product (Fig. S5) in both dry and humid conditions. For butanal increasing the temperature increased the amount of water loss product ion formed in the H_3O^+ channel (Fig. S7) but only had minor impacts on the NO^+ (Fig. S8) and O_2^+ (Fig. S9) channel under dry conditions. Increasing the flow tube voltage increased fragmentation of the primary product ion to further promote the water loss product in the H_3O^+ channel, promote the formation of the $C_3H_7^+$ product ion in the NO^+ channel and
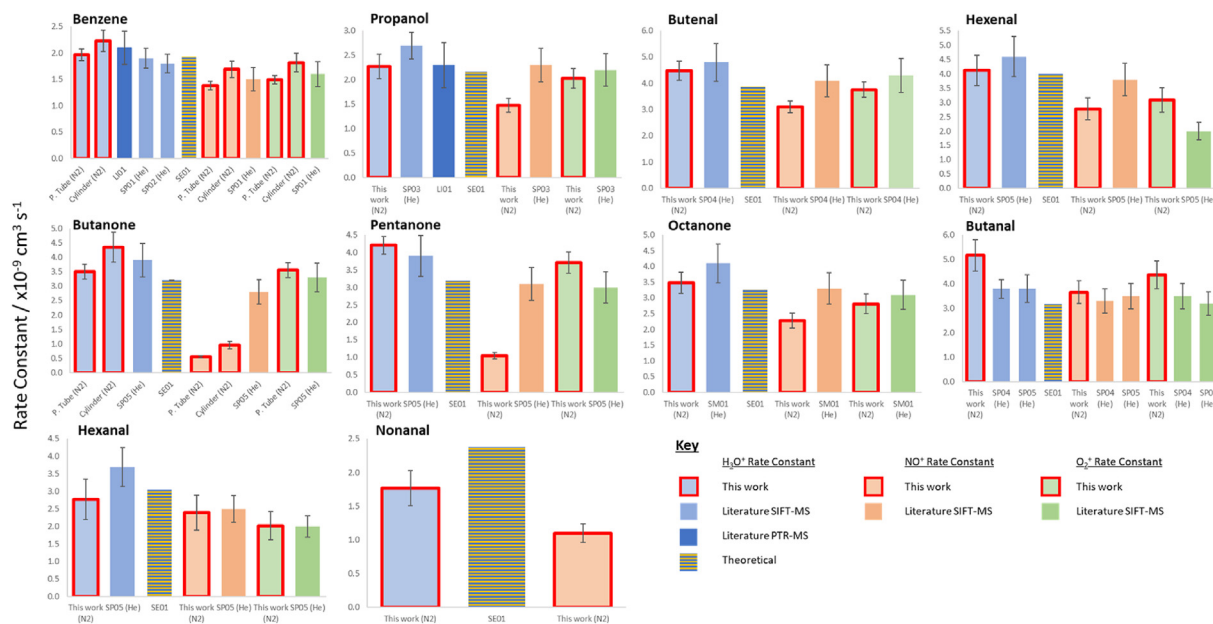
Fig. 4. Comparison of rate constants measured in this study with those of Lindinger et al. [72] (LI01), Spanel et al. [61] (SP01), Spanel et al. [62] (SP02), Sekimoto et al. [73] (SE01), Spanel et al. [54] (SP03), Spanel et al. [63] (SP04), Spanel et al. [53] (SP05) and Smith et al. [64] (SM01). For benzene and butanone *P. Tube* represents the permeation tube measurement and *Cylinder* represents the calibration cylinder measurement.

form it in the O$_2^+$ channel. Under humid conditions the increase in temperature removes the primary water adduct product ion in both the H$_3$O$^+$ and NO$^+$ channels. The increase in flow tube voltage has a similar impact under dry conditions for both the H$_3$O$^+$ and NO$^+$ channels and introduces more fragmentation in the O$_2^+$ channel. For butanone the increase in temperature has no impact on the ion distribution under either dry or humid conditions and the increase in voltage causes slight fragmentation in the dry H$_3$O$^+$ (Fig. S11) and NO$^+$ (Fig. S12) channels as well as in both dry and humid O$_2^+$ (Fig. S13) channels.

2.3. Determination of product ion m/z's

Full mass scans were performed on each compound to determine the product ions to be measured in selected ion monitoring (SIM) mode, with an ion dwell limit per *m/z* of 100 ms, count limit per *m/z* of 10,000 counts and repeats over a range of 18−400 *m/z* in steps of 1 *m/z*. The flow tube temperature of the SIFT-MS was held at 140 °C with a flow tube pressure of 460 mTorr. Blanks were measured by flowing 0.01 slpm (standard litres per minute) of N$_2$ diluent gas past the SIFT-MS which sampled at 25 sccm. The main run was performed the same way, but with the permeation oven outflow on. The average of the last five blank measurements at each *m/z*, for each reagent ion, was subtracted from the corresponding value for the non-blank signal to give a blank corrected spectrum from which the product ions were determined. The scans were run at 0.01 slpm diluent flow to introduce as large a possible concentration into the SIFT-MS, allowing all product ions to be easily identifiable as well as any ions arising from secondary chemistry.

2.4. Determination of rate constants and branching ratios

For determination of rate constants, a number of SIM mode scans were run per compound. This used a method identical to that of the full scan method, except with 401 repeats, at a measurement time limit per *m/z* of 100 ms and an ion dwell limit per *m/z* of 10,000 counts, of the H$_3$O$^+$ (*m/z* 19, 37 and 55), NO$^+$ (*m/z* 30) and

O$_2^+$ (*m/z* 32) reagent ions and the required *m/z* values of the product ions for the compound. These scans were run over a range of diluent flows to allow the rate constant to be calculated over a range of concentrations. From these runs the last 400 repeats were averaged for each ion in both the blank and non-blank mass spectra. After the removal of outliers, the blank average was subtracted from the non-blank average to give a final run ion count for each measured ion. The branching ratio for each product ion was calculated from this data by dividing the individual product ion count at each *m/z* by the total product ion count.

Properties like the carrier flow rate, flow tube temperature and flow tube pressure were averaged over the two runs, which varied by a maximum of 0.05%. The rate constant, k_i, for each reagent ion, *i*, reacting with a compound can be calculated as [71];

$$k_i = \frac{\left(\frac{-dN_i}{dt}\right)}{N_i C_j} \tag{1}$$

where $-dN_i$ is the reduction in reagent counts (essentially the sum of the product ion counts) in counts per second (cps), *dt* is the reaction time (recorded by the instrument) in s, N_i is the total reagent ion count (taken from the blank) in cps and C_j is the concentration of the compound, taking into account its dilution by the diluent and SIFT-MS carrier gas flow, in molecules cm^{-3}. The rate constant was determined by plotting $-dN_i/dt$ vs. $N_i C_j$.

The branching ratio was calculated as;

$$BR_x = \frac{N_x}{N_p} \times 100$$

where BR_x is the branching ratio of product ion *x* (as a percentage), N_x is the product ion count of *x* and N_p is the total product ion count for all product ion in the reagent ion channel the branching ratio is being calculated for. These branching ratios are useful for both individual compound quantitation, alongside the rate constant, and for method development. It is important to know all product ions that occur for compounds expected in a mixture to ensure no

overlapping peaks are used as this ensures reliable quantitation of concentration. Isotopologues are not measured in this work due to their low abundance relative to the major product ions. The contributions of isotopologues to the product ions are much smaller than other uncertainties such as those associated with calibration, which are described below.

3. Results and discussion

3.1. Permeation data

Calculated mixing ratios of all analytes supplied from the permeation tube calibration system are shown in Table 1. The error of the final mixing ratios were calculated as follows.

The error in the mixing ratio emitted from the permeation tube, Err_{Cperm}, is calculated as;

$$Err_{C_{perm}} = C_{perm} \sqrt{\left(\frac{Err_T}{T}\right)^2 + \left(\frac{Err_m}{m}\right)^2 + \left(\frac{Err_V}{V}\right)^2} \qquad (2)$$

where Err_T is the measurement accuracy of the temperature controller (0.5 K), Err_m is the error of the mass loss from the permeation tube, calculated from the slope error, and Err_v is the error of the flow rate over the permeation tubes (0.8% reported by Alicat).

The error in the mixing ratio delivered to the SIFT after all dilution steps, Err_{CSIFT}, is calculated as;

$$Err_{C_{SIFT}} = C_{SIFT} \sqrt{\left(\frac{Err_{C_{perm}}}{C_{perm}}\right)^2 + \left(\frac{Err_{Q_{carrier}}}{Q_{carrier}}\right)^2 + 2\left(\frac{Err_{Q_{sample}}}{Q_{sample}}\right)^2 + x\left(\frac{Err_{Q_{perm}}}{Q_{perm}}\right)^2} \qquad (3)$$

where $Err_{Qcarrier}$ is the error in the carrier gas flow, calculated from the standard deviation of measurements of the carrier flow in the blank and analyte runs, $Err_{Qsample}$ is the error in the sample inlet flow (0.8%, Alicat), multiplied by two for the blank and measurement, Err_{Qperm} is the error in the flow rate through a single permeation oven and x is the number of permeation oven flows used. Further detail on the error calculation is given in the supplementary information.

In Table 1 the R^2 value represents how well the mass loss over time fits a straight line and is therefore a measure of the precision of the calculated mixing ratios.

3.2. SIFT-MS data

3.2.1. Rate data

The measured rate constants are shown in Table 2 and compared to previously published rate constants in Fig. 4.

The error in the measured rate constants reported in Table 2 and shown in Fig. 4, Err_k, was calculated as;

$$Err_k = k \sqrt{\left(\frac{Err_{C_{SIFT}}}{C_{SIFT}}\right)^2 + \left(\frac{Err_{dN_i}}{dN_i}\right)^2 + \left(\frac{Err_{N_i}}{N_i}\right)^2} \qquad (4)$$

where Err_{CSIFT} is the error in the mixing ratio delivered to the SIFT, Err_{Ni} is the error in the reagent ion count, calculated as the standard deviation of all measurements of the reagent ion in the blank, and Err_{dNi} is the error in the total product ion count, calculated as the root sum square of the errors of each individual product ion count contributed by the both the analyte measurement and the corresponding blank.

3.2.1.1. Benzene. For benzene, the nitrogen H_3O^+ rate constant measured here was within 3.6% of that measured by Spanel et al. [61] (herein referred to as SP01) and within 8.6% of that measured by Spanel et al. [62] (herein referred to as SP02), both measured in helium. The measured H_3O^+ rate constant was also comparable to a PTR-MS rate constant measured by Lindinger et al. [72] (herein referred to as LI01) and a theoretical rate constant as calculated by Sekimoto et al. [73] (herein referred to as SE01). The nitrogen NO^+ and O_2^+ rate constants measured were also comparable with those measured by SP01 (within 8.7% and 7.4% respectively).

3.2.1.2. 1-Propanol. The measured propanol rate constants in nitrogen are similar to previous data reported by Spanel et al. [54] (herein referred to as SP03) for both H_3O^+ (within 15.9%) and O_2^+ (within 7.7%) in helium, but the NO^+ rate constant is 35.7% lower than that reported by SP03 in helium. This pattern is also seen for other compounds in this study where the NO^+ rate constant measured is smaller than those reported in the literature, but the H_3O^+ or O_2^+ rate constants remain similar. The H_3O^+ rate constant also compares well to a PTR-MS rate constant reported by LI01 and a calculated rate constant via SE01.

Table 1
Calculated mixing ratios for all permeation tubes used in this study.

Compound		Mixing Ratio / ppb		Measurements	Holding Temperature / °C	R [2]
Name	Formula	Value	% Error			
Benzene	C_6H_6	2759	0.91	25	40	1.000
1-Propanol	C_3H_8O	284.8	3.77	12	40	0.987
Butanal	C_4H_8O	5035	2.52	10	40	0.996
2-Butanone	C_4H_8O	2641	1.03	10	40	1.000
2-Butenal	C_4H_6O	5006	1.61	8	40	0.999
2-Pentanone	$C_5H_{10}O$	1023	1.06	14	40	1.000
Hexanal	$C_6H_{12}O$	764.5	8.09	15	50	0.926
2-Hexenal	$C_6H_{10}O$	970.0	5.40	14	50	0.968
2-Octanone	$C_8H_{16}O$	230.4	3.46	12	50	0.989
Nonanal	$C_9H_{18}O$	371.0	3.43	8	70	0.994

The permeation tube systems provided stable concentrations of all the compounds, with an average calculated mixing ratio uncertainty of 3.1%.

Table 2
Measured and literature rate constants and branching ratios. Branching ratio percentages under 10% have been removed for clarity.

Compound	Work	Temperature / °C	Carrier Gas	Source	H_3O^+ Rate / $\times10^{-9}$ cm^3 s^{-1}	Ion / m/z	Ratio / %	NO^+ Rate / $\times10^{-9}$ cm^3 s^{-1}	Ion / m/z	Ratio / %	O_2^+ Rate / $\times10^{-9}$ cm^3 s^{-1}	Ion / m/z	Ratio / %
Benzene	This work	140	N_2	Permeation Tube	2.0 ± 0.1	79	100	1.4 ± 0.1	78	93	1.5 ± 0.1	78	100
	This Work	140	N_2	Cylinder	2.2 ± 0.2	79	100	1.7 ± 0.2	78	93	1.8 ± 0.2	78	100
	SP01	Room Temperature	He	Plastic Bag	1.9 ± 0.4	79	100	1.5 ± 0.3	78 108	85 15	1.6 ± 0.3	78	100
	SP02	Room Temperature	He	Plastic Bag	1.8 ± 0.4	79	100	N/A	N/A	N/A	N/A	N/A	N/A
1-propanol	This work	140	N_2	Permeation Tube	2.3 ± 0.3	43	100	1.5 ± 0.1	59	100	2.0 ± 0.2	31 42 59	67 13 20
	SP03	Room Temperature	He	Plastic Bag	2.7 ± 0.5	43 61	90 10	2.3 ± 0.4	59	100	2.2 ± 0.4	42 55	10 90
Butanal	This work	140	N_2	Permeation Tube	5.2 ± 0.6	55 73	89 11	3.7 ± 0.5	43 71	75 25	4.4 ± 0.6	43 44 57 72	17 48 13 23
	SP04	Room Temperature	He	Plastic Bag	3.8 ± 0.8	73	95	3.3 ± 0.7	71	100	3.2 ± 0.6	44 72	50 50
	SP05	Room Temperature	He	Plastic Bag	3.8 ± 0.8	73	95	3.5 ± 0.7	71	100	3.5 ± 0.7	44 72	65 35
Butanone	This work	140	N_2	Permeation Tube	3.5 ± 0.3	73	100	0.6 ± 0.0	102	97	3.6 ± 0.3	29 43 57 72	12 43 26 18
	This work	140	N_2	Cylinder	4.4 ± 0.5	73	100	1.0 ± 0.1	102	92	N/A	N/A	N/A
	SP05	Room Temperature	He	Plastic Bag	3.9 ± 0.8	73	100	2.8 ± 0.5	102	100	3.3 ± 0.6	43 57 72	40 25 35
Butenal	This work	140	N_2	Permeation Tube	4.5 ± 0.4	71	100	3.1 ± 0.2	69	95	3.7 ± 0.3	42 69 70	18 52 20
	SP04	Room Temperature	He	Plastic Bag	4.8 ± 0.9	71	100	4.1 ± 0.8	69	100	4.3 ± 0.9	69 70	65 30
Pentanone	This work	140	N_2	Permeation Tube	4.2 ± 0.3	45 87	27 73	1.1 ± 0.1	116	100	3.7 ± 0.3	43 58 71 86	47 27 13 13
	SP05	Room Temperature	He	Plastic Bag	3.9 ± 0.8	87	100	3.1 ± 0.6	116	100	3.0 ± 0.6	43 58 71 86	50 20 15 15
Hexanal	This work	140	N_2	Permeation Tube	2.8 ± 0.6	55 83 101	22 59 15	2.4 ± 0.5	43 71 99	26 37 32	2.0 ± 0.4	44 56 57 82	32 35 14 10
	SP05	Room Temperature	He	Plastic Bag	3.7 ± 0.7	83 101	50 50	2.5 ± 0.5	99	100	2.0 ± 0.4	44 56	30 50
Hexenal	This work	140	N_2	Permeation Tube	4.1 ± 0.5	57 99	56 36	2.8 ± 0.4	55 97	33 64	3.1 ± 0.4	43 69 83 98	15 10 11 24
	SP05	Room Temperature	He	Plastic Bag	4.6 ± 0.9	99	100	3.8 ± 0.8	71 97	15 85	3.7 ± 0.7	43 69 70 98	30 30 20 20
Octanone	This work	140	N_2	Permeation Tube	3.5 ± 0.3	129	100	2.3 ± 0.2	158	100	2.8 ± 0.3	58 59 128	51 18 12
	SM01	Room Temperature	He	Plastic Bag	4.1 ± 0.8	129	100	3.3 ± 0.6	158	100	3.1 ± 0.6	58 59 128	50 15 30
Nonanal	This work	140	N_2	Permeation Tube	1.8 ± 0.3	57 69 83 143	18 34 11 28	1.1 ± 0.1	57 71 141	29 16 54	N/A	N/A	N/A

3.2.1.3. Butenal.

The Butenal rate constants for H_3O^+, NO^+ and O_2^+ are all within error of those measured by Spanel et al. [63] (herein referred to as SP04) in helium. The NO^+ rate constant we measure is only just within the error of the measurement by SP04, at 3.1×10^{-9} cm^3 s^{-1} compared to 4.1×10^{-9} cm^3 s^{-1}.

3.2.1.4. Hexenal. The hexenal rate constants for all reagent ions are all within error of those measured by Spanel et al. [53] (herein referred to as SP05) in helium. Both unsaturated aldehydes produced similar results with an H_3O^+:NO^+ rate constant ratio of 1.44:1.00 for butenal and 1.48:1.00 for hexenal. These similar ratios are an indication that unsaturated aldehydes have a similar rate constant ratio trend.

3.2.1.5. Butanone. The butanone rate constants for H_3O^+ and O_2^+ were comparable to those measured in SP05 in helium. The NO^+ rate constant we measured was much lower than that measured in SP05, 0.6×10^{-9} cm^3 s^{-1} compared to 2.8×10^{-9} cm^3 s^{-1}, a reduction of almost 80%. The calibration gas cylinder containing benzene and 2-butanone was also measured to confirm the lower NO^+ rate constant was not an artefact of the permeation tube source. The benzene rate constants were close to the measured permeation tube rate constants and the literature for all three reagent ions, confirming that the cylinder measurement NO^+ rate constant of 1.0×10^{-9} cm^3 s^{-1} for 2-butanone was valid. The calibration cylinder measurement is much closer to our permeation tube measurement of 0.6×10^{-9} cm^3 s^{-1} than the value measured in SP05. The theoretical rate constant calculated in SE01 for the H_3O^+ rate constant was lower than that measured in this study.

3.2.1.6. Pentanone. As with butanone, the pentanone rate constants were comparable to those measured in SP05 in helium and the NO^+ rate constant measured was much lower than that measured in SP05. The NO^+ rate constant measured was 1.1×10^{-9} cm^3 s^{-1} compared to 3.1×10^{-9} cm^3 s^{-1} in SP05, a reduction of around 65%. The theoretical rate constant calculated in SE01 for the H_3O^+ rate constant was lower than that measured in this study.

3.2.1.7. Octanone. For octanone, the NO^+ value we measured in nitrogen was closer than the other two compounds to the value measured by Smith et al. [64] (herein referred to as SM01) in helium, 2.3×10^{-9} cm^3 s^{-1} compared to 3.3×10^{-9} cm^3 s^{-1}, a reduction of around 30% and just outside the error range. The H_3O^+ and O_2^+ rate constants measured were both close to the values reported in SM01. The theoretical rate constant calculated in SE01 for the H_3O^+ rate constant was lower than that measured in this study.

3.2.1.8. Butanal. The butanal rate constants measured in nitrogen were all higher than those reported in SP04 and SP05 in helium, though the NO^+ and SP04 O_2^+ rate constants were within the error of our measured values. The H_3O^+ rate constant measured was especially high, 5.2×10^{-9} cm^3 s^{-1} compared to 3.8×10^{-9} cm^3 s^{-1} reported in both SP04 and SP05. This was also higher than the calculated SE01 theoretical rate constant.

3.2.1.9. Hexanal. The nitrogen measured hexanal rate constants for NO^+ and O_2^+ compare well with SP05 helium-based rate constants but the H_3O^+ rate constant is lower, although just within the error of the SP05 value, 2.8×10^{-9} cm^3 s^{-1} compared to 3.7×10^{-9} cm^3 s^{-1}, and was similar to the SE01 derived rate constant.

3.2.1.10. Nonanal. There is no literature comparison for nonanal, except for a theoretical SE01 value at 2.4×10^{-9} cm^3 s^{-1} which is higher 30% than our measured 1.8×10^{-9} cm^3 s^{-1}.

3.2.1.11. Overview of rate constant data. The most significant differences between our measurements and previous studies all occur for compounds with only a single adduct product, namely the NO^+ ketone rate constants. This likely suggests that the collision complex is being formed but is not effectively stabilised in our higher energy system compared to previous measurements. Alternatively, there could be a region where these ions are undergoing collisions that could destroy the adduct complex. This was also seen in the temperature and voltage experiments in Section 2.2 which confirmed that both increasing the flow tube temperature and flow tube voltage decrease the sensitivity of NO^+ adduct formation which would reduce the rate constant as we see in our results.

3.2.2. Product ions and branching ratios

3.2.2.1. Benzene. The product ions for benzene match those observed in SP01. The only H_3O^+ product appears at m/z 79 which is the proton transfer product of benzene as shown in (R1).

$$C_6H_6 + H_3O^+ \rightarrow C_6H_6H^+ + H_2O \quad (R1)$$
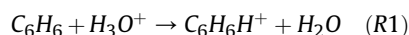
There are two NO^+ products that form which are the same in our study and that of SP01. These are a charge transfer product appearing at m/z 78 (R2) and an NO adduct at m/z 108 (R3). In the SP01 study, the charge transfer product to NO adduct branching ratio was 85:15, but we observed a branching ratio of 93:7. The higher charge transfer product found in our work is due to a combination of the higher flow tube temperature and increased flow tube voltage used in our measurements that increase the total energy in the system. At higher energy the adduct decomposes at a greater rate leading to a decreased percentage of the adduct.

$$C_6H_6 + NO^+ \rightarrow C_6H_6^+ + NO \quad (R2)$$

$$C_6H_6 + NO^+ \rightarrow C_6H_6.NO^+ \quad (R3)$$
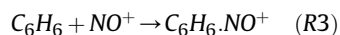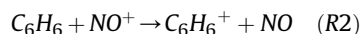
The O_2^+ product ion at m/z 78, formed by a charge transfer reaction (R4), is the same in both our work and the Smith et al. [61] work. This is the only product formed.

$$C_6H_6 + O_2^+ \rightarrow C_6H_6^+ + O_2 \quad (R4)$$
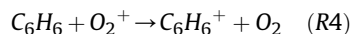
3.2.2.2. 1-Propanol. For the reaction of propanol with H_3O^+ we only detected the m/z 43 product ion, derived from the loss of water following proton transfer (R5), a common mechanism in alcohols and aldehydes.

$$C_3H_7OH + H_3O^+ \rightarrow C_3H_7OHH^+ + H_2O \rightarrow C_3H_7^+ + H_2O \quad (R5)$$
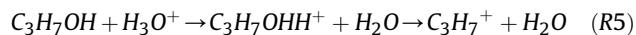
SP03 observed an additional product ion for this reaction at m/z 61, although the m/z 43 product ion was favoured with a branching ratio of 90:10. It is possible that the higher energy in our SIFT caused the loss of water to become even more favourable than found in the SP03. The NO^+ product ion at m/z 59 appears as the only NO^+ product ion of propanol in both our study and SP03. The m/z 59 ion is formed via hydride transfer as shown in (R6).

$$C_3H_7OH + NO^+ \rightarrow C_3H_7O^+ + HNO \quad (R6)$$
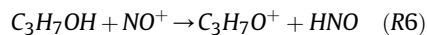
The O_2^+ product ions in our study are the same as those observed in SP03 [54] but we also observed a product ion at m/z 59, equivalent to the loss of a hydrogen atom. The other two product ions are m/z 31 and m/z 42, both breakdown products after charge transfer and formed from the loss of an ethyl group and a water molecule, respectively. While the m/z 31 ion remains the major product ion in our measurements, the ratios, with the addition of the m/z 59 ion, are quite different from those observed by SP03. We measure a branching ratio of 67:13:20 (m/z 31:42:59) compared to SP03 of 90:10 (m/z 31:42).

3.2.2.3. Butenal. The observed butenal product ions match those reported in SP04 closely. The major H_3O^+ product is the proton transfer product at *m/z* 71. We observed an extra product ion at *m/z* 43, though at an extremely low ion count of 0.2%, which could be treated as insignificant. The major NO^+ product ion is that resulting from hydride transfer at *m/z* 69. Another product ion appears at *m/z* 41 that was not shown by SP04 [63]. This ion is formed from fragmentation after the hydride transfer forming either C_2HO^+ or $C_3H_5^+$ at a branching ratio of 5.4%. We detected all the SP04 product ions; *m/z* 70, the charge transfer product, *m/z* 69, a hydride transfer product, and *m/z* 42 ($C_3H_6^+/C_2H_2O^+$), a fragment ion. We observed two more minor fragment ions at *m/z* 55 ($C_3H_3O^+$) and *m/z* 41 ($C_2HO^+/C_3H_5^+$) and observed a higher proportion of butenal fragment ions, with only 72% of the product ion resulting from charge transfer or hydride transfer, compared to 95% in SP04.

3.2.2.4. Hexenal. The hexenal product ions detected were quite different to those observed in SP05. The proton transfer product, *m/z* 99, which was the only product ion reported by SP05, only accounted for 35% of our observed product ion count, instead the major product ion was a fragmentation product at *m/z* 57 ($C_4H_9^+$ - 53%) with a minor water loss product ion at *m/z* 81 (8%). The NO^+ hydride transfer product at *m/z* 99 was detected in both our work and SP05. In SP05 a fragment ion at *m/z* 71 ($C_4H_7O^+$ - 15%) was observed which we did not detect, though we did detect fragment ions at *m/z* 55 ($C_2H_2O^+$ - 31%) and *m/z* 69 ($C_4H_5O^+/C_5H_9^+$ - 2.8%). We observed more numerous O_2^+ product ions than those observed by SP05, who observed the charge transfer product, *m/z* 98 ($C_6H_{10}O^+$ - 20%), and three fragment ions, *m/z* 70 ($C_4H_6O^+$ - 20%), *m/z* 69 ($C_5H_9^+/C_4H_5O^+$ - 30%) and *m/z* 43 ($C_2H_3O^+/C_3H_7^+$ - 30%). These product ions only make up 53.2% of our product ion count, with eight more product ions accounting for the remaining 46.8%. The charge transfer ion is the only product ion that increases in branching ratio, from 20% to 24%, whereas the remaining fragment ions have a range of 2.8%–14.5%. This difference is possibly due to the increased energy in our system causing much greater fragmentation compared to SP05. The SP05 data for hexenal was observed using a He carrier gas, whereas our measurements use N_2, which may also influence the product ions formed.

3.2.2.5. Butanone. The butanone product ions observed here are similar to those observed in SP05. The only H_3O^+ product ion observed in both our work and SP05 is the proton transfer product, *m/z* 73 ($C_4H_9O^+$). The NO^+ product ions are also similar. The major product ion we observed was the NO adduct at *m/z* 102 ($C_4H_8 \cdot NO^+$ - 97%), which was the only one observed in SP05, but we also observed a minor charge transfer product at *m/z* 72 ($C_4H_8O^+$ - 3%). The O_2^+ product ions were also similar, with only one more fragment ion observed in our work compared to SP05. We detected a lower fraction of the charge transfer product at *m/z* 72 ($C_4H_8O^+$ - 18%) than SP05 and observed similar amounts of the fragment ions at *m/z* 57 ($C_3H_5O^+$ - 26%) and *m/z* 43 ($C_2H_3O^+$ - 43%) as well as an additional fragment ion at *m/z* 29 ($C_2H_5^+/CHO^+$ - 12%).

3.2.2.6. Pentanone. In agreement with SP05, the major pentanone H_3O^+ product ion observed was the proton transfer product at *m/z* 87 ($C_5H_{10}OH^+$ - 73%). However, we also observed a fragment ion at *m/z* 43 ($C_2H_3O^+/C_3H_7^+$ - 27%). The NO^+ product ion observed, by both us and SP05, is the NO adduct at *m/z* 116 ($C_5H_{10}O \cdot NO^+$ - 100%). All observed O_2^+ product ions are the same as those in SP05, at similar branching ratios, the charge transfer ion at *m/z* 86 ($C_5H_{10}O^+$ - 13%) and the fragment ions at *m/z* 71 ($C_4H_7O^+$ - 13%), *m/z* 58 ($C_3H_6O^+$ - 27%) and *m/z* 43 ($C_2H_3O^+/C_3H_7^+$ - 47%).

3.2.2.7. Octanone. The octanone H_3O^+ and NO^+ product ions

observed match those observed by SM01 with the H_3O^+ proton transfer ion at *m/z* 129 ($C_8H_{16}OH^+$ - 100%) and the NO^+ NO adduct at *m/z* 158 ($C_8H_{16}O \cdot NO^+$ - 100%). The O_2^+ product ions mostly match SM01, with similar branching ratios. The charge transfer product at *m/z* 128 ($C_8H_{16}O^+$ - 12%) and fragment ions at *m/z* 113 ($C_7H_{13}O^+$ - 5%), *m/z* 85 ($C_6H_{13}^+$ - 7%), *m/z* 71 ($C_5H_{11}^+$ - 7%), *m/z* 59 ($C_3H_7O^+$ - 18%), *m/z* 58 ($C_3H_6O^+$ - 51%). The fragment ion at *m/z* 113 is not observed by SM01 and they measure a fragment at *m/z* 43 that we don't observe.

3.2.2.8. Butanal. The butanal H_3O^+ product ions observed by SP05 match those we observed, though we observed more of the proton transfer product, at *m/z* 73 ($C_4H_8OH^+$ - 11%), and less of the proton transfer water loss product, at *m/z* 55 ($C_4H_7^+$ - 89%). For NO^+, we observed a different major product ion at *m/z* 43 ($C_2H_3O^+/C_3H_7^+$ - 75%) in addition to the hydride transfer product at *m/z* 71 ($C_4H_7O^+$ - 25%) reported by SP05. We observed a fragment ion at *m/z* 43 ($C_2H_3O^+/C_3H_7^+$ - 47%) and two additional fragment ions in the O_2^+. We observed the charge transfer ion, at *m/z* 72 ($C_4H_8O^+$ - 22%), a fragment ion, at *m/z* 44 ($C_2H_4O^+$ - 46%), and additional fragment ions at *m/z* 57 ($C_3H_5O^+$ - 12%) and at *m/z* 43 ($C_2H_3O^+/C_3H_7^+$ - 16%).

3.2.2.9. Hexanal. The hexanal H_3O^+ product ions we measure are similar to those we measure for pentanal. We observed the proton transfer product, at *m/z* 101 ($C_6H_{12}O^+$ - 15%), and proton transfer water loss product, at *m/z* 83 ($C_6H_{11}^+$ - 59%), as well as two extra fragment ions at *m/z* 69 ($C_4H_5O^+/C_5H_9^+$ - 4.7%) and *m/z* 55 ($C_4H_7^+/C_3H_3O^+$ - 22%). The NO^+ product ions consisted of the hydride transfer ion observed by SP05, at *m/z* 99 ($C_6H_{11}O^+$ - 32%), and multiple fragment ions, that SP05 didn't measure, at *m/z* 85 ($C_5H_9O^+$ - 2%), *m/z* 71 ($C_4H_7O^+$ - 37%), *m/z* 57 ($C_3H_5O^+$ - 4%) and *m/z* 43 ($C_2H_3O^+$ - 26%). The O_2^+ product ions were mostly similar to SP05 [53], with one fragment ion missing, *m/z* 97. We observed an additional fragment at *m/z* 82 ($C_5H_6O^+/C_6H_{10}$ - 10%) in addition to fragments at *m/z* 72 ($C_5H_{12}^+$ - 9%), *m/z* 57 ($C_3H_5O^+$ - 14%), *m/z* 56 ($C_3H_4O^+$ - 35%) and at *m/z* 44 ($C_2H_4O^+$ - 32%) that were also observed in SP05.
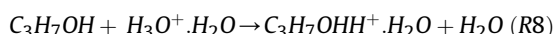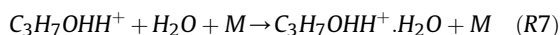
3.2.2.10. Nonanal. We observed the proton transfer product for nonanal at *m/z* 143 ($C_9H_{19}O^+$ - 28%) and the water loss product at *m/z* 125 ($C_9H_{17}^+$ - 9%) for the H_3O^+ reagent ion. We also observed three fragment ions at *m/z* 83 ($C_6H_{11}^+$ - 11%), *m/z* 69 ($C_4H_5O^+/C_5H_9^+$ - 34%) and *m/z* 57 ($C_4H_9^+$ - 18%). With the NO^+ reagent ion nonanal formed the hydride transfer product at *m/z* 141 ($C_9H_{15}O^+$ - 54%) and two fragment ions at *m/z* 71 ($C_4H_7O^+$ - 16%) and *m/z* 57 ($C_3H_5O^+$ - 29%). There were no literature references to compare these measurements to.

3.2.2.11. Overview of product ions and branching ratios. A major feature of many our results compared to those reported in the literature is the greater proportion of fragmentation in our measurements, especially in larger compounds. This is due to a combination of the increased flow tube temperature of 140 °C and the increased flow tube voltage increasing the overall energy in the system, leading to greater fragmentation. The temperature of our flow tube is close to the standard operating temperature (120 °C) of the Voice200*ultra*. The measurements referenced above (SP01-05 and SM01) were performed at 'room temperature'. We increased the flow tube temperature to limit the impact of humidity on the product ions, especially when measuring at humid conditions. The flow tube voltage change from 25 V to 50 V also increases the energy in the reagent ions by increasing the energy gradient through the flow tube. This will accelerate the reagent ions in our instrument faster relative to the reagent ions in a standard Voice200*ultra*, increasing the amount of fragmentation. The fragmentation was so

great in the larger chain aldehydes that the O_2^+ spectra were not observed as the spectra produced were so complex.

3.2.3. Secondary product ions formed under humid conditions

We define 'humid product ions' as any product ion that is formed in the humid full scan that is not shown in the dry full scan. These 'humid product ions' consist of single, double and triple water adducts of the dry product ion. An example of the formation of a water adduct in the reaction of propanol with H_3O^+ in humid air is shown below in R7 (where $C_3H_7OHH^+$ is formed in R5) and R8, where M is a third body like N_2;

$$C_3H_7OHH^+ + H_2O + M \rightarrow C_3H_7OHH^+.H_2O + M \quad (R7)$$

$$C_3H_7OH + H_3O^+.H_2O \rightarrow C_3H_7OHH^+.H_2O + H_2O \quad (R8)$$

It is important to measure the impacts of humidity as many environmental samples will have varying humidity levels. Being able to accurately identify and quantify compounds over a range of environmental conditions is important for the widespread use of the SIFT-MS technique. Measurements of humid product ions have been made before. Spanel et al. [55] observed a mixture of primary alcohols (C_2-C_6) over a sample gas humidity range 1−5.5%. In their study they find the ratio of the H_3O^+ reagent ion to its water adducts, $H_3O^+(H_2O)_{1,2,3}$, to be 70:18:9:4 at 1.6% humidity and 29:14:19:38 at 5.5% humidity. In our study we observed H_3O^+ and its water adducts to be 40:60:0:0 at relative humidities ranging from 38 to 83%. This suggests that the ion energies are sufficiently high at the higher flow tube temperature used here (we run at 140 °C in nitrogen compared to Spanel et al. [55] of 27 °C in helium) that water clusters greater than one water molecule are readily fragmented, if formed at all. Spanel et al. [55] also observed NO^+ and its primary and secondary water clusters to be 98.4:1.5:0.1 at 1.6% humidity and 94.6:4.3:1.1 at 5.5% humidity whereas we measure only the dry NO^+ reagent ion at 100% across all observed humidities.

For a limited number of compounds we were able to measure additional product ions formed under conditions of high humidity. The method required humidifying the diluent line and so to achieve the higher relative humidities (e.g. 80%) a high diluent flow was required. This meant that ion counts for the low mixing ratio compounds (1-propanol, octanal, 2-octanone, nonanal and decanal) were too low for any meaningful measurement. For benzene, 2-butenal, 2-hexenal, 2-butanone, 2-pentanone, butanal, pentanal and hexanal ion counts were sufficiently high to determine ions formed from the introduction of humidity as shown in Table 3.

No 'humid product ions' were detected for any compound in the H_3O^+ channel, this could be due to the high tube temperature

(140 °C). This is unusual as studies like those of Spanel et al. [55] and Smith et al. [74] have shown the prevalence of humid product ions for reactions of OVOCs with the H_3O^+ reagent ion under wet conditions. This further supports the theory that the energy in the system may be responsible for adduct breaking. Spanel et al. [55] found the maximum percentage for the dry product ions for methanol, at an absolute humidity of 1.6%, to be 43%, with the remaining 57% to be made up of the primary and secondary water clusters. They even found that for their largest alcohol, hexanol, at the lowest absolute humidity, 1.6%, only 90% of the product was attributable to dry product ions, the remaining 10% due to the primary and secondary water clusters. Smith et al. [74] found similar results for aldehydes. The highest proportion of dry product ions was observed for ethanal, at 2% absolute humidity, with only 53% of the product ion resulting from the dry product ion.

Benzene formed no humid product ions at all in our system. Warneke et al. [75] also found no humid product ions when measuring benzene over a range of humidities by PTR-MS, as expected as at normal E/N values there would be enough energy to fragment them.

Except for butenal and pentanone, the proportion of humid product ions as a percentage of the total product ion count was relatively low, which we attribute to the higher temperature of our flow tube, resulting in only a small impact of humidity on the final ion distribution. Most of the humid product ions increased as a proportion of the total ion count with increasing humidity but there were a couple that did not, these being the butanal and pentanal humid product ions as well as the pentanone m/z 89 humid product ion.

For Butenal, humid product ions accounted for 0.5−1.8% of the NO^+ product ions and 14.0−20.5% of the O_2^+ product ions over a range of relative humidities from 37.5 to 83.3%. The humid product ions here are primary water clusters of the each of the product ions, e.g. the NO^+ hydride transfer product at m/z 69 forms a water cluster ion at m/z 87 $C_4H_5O^+.H_2O$.

For pentanone a humid product ion appeared at m/z 87 which cannot be assigned to a water cluster of a dry product ion. It is uncertain what this product ion is, but it appears in all humid spectra of the pentanone permeation tube and the proportion of the product ion increases with increasing humidity.

4. Conclusions

We present rate constants and branching ratios for a range of OVOC compounds measured by SIFT-MS under conditions designed to maximise the sensitivity and decrease the formation of water clusters when measuring humid samples, namely a flow tube temperature of 140 °C and alterations to the lens voltages

Table 3
The humid product ions of all compounds measured in this study reported as a percentage of the entire product ion count for each reagent ion. Humidities ranged from 37.5 to 83.3%.

Compound	NO^+			O_2^+		
	Ion	Formula	% Ion Count	Ion	Formula	% Ion Count
Benzene	−	−	−	−	−	−
2-Butenal	87	$C_4H_5O^+(H_2O)$	0.5−1.8	87	$C_4H_5O^+(H_2O)$	1.2−2.9
	88	$C_4H_6O^+(H_2O)$	0.0−0.1	88	$C_4H_6O^+(H_2O)$	13.4−19.2
2-Hexenal	115	$C_6H_9O^+(H_2O)$	0.1−0.4	−	−	−
2-Butanone	−	−	−	61	$C_2H_3O^+(H_2O)$	0.0−8.0
				62	$C_2H_4O^+(H_2O)$	0.0−0.2
2-Pentanone	−	−	−	87	??	11.0−15.2
				89	$C_4H_7O^+(H_2O)$	0.4
Butanal	89	$C_4H_7O^+(H_2O)$	3.7	75	$C_3H_5O^+(H_2O)$	0.2
Pentanal	103	$C_5H_9O^+(H_2O)$	25.9	−	−	−
Hexanal	−	−	−	−	−	−

compared to standard operating conditions. We also used nitrogen rather than helium carrier gas; this is becoming an increasingly common practice in many analytical techniques due to the dwindling supply of helium and associated rising costs. We show that using nitrogen carrier gas coupled with changed flow tube conditions to better control humidity dependence and increase sensitivity has a noticeable impact on some rate constants, especially reactions with the NO^+ reagent ion where an adduct is formed. This is particularly noticeable for ketones where NO^+ rate constants in nitrogen carrier gas were up to a factor of 5 lower than those previously measured in helium. We suggest this is due to the increased flow tube temperature and voltage as demonstrated by the data presented in Section 2.2 and in the supplementary data.

The branching ratios measured in this study were markedly different to those measured previously. Ion energies in the SIFT-MS, and therefore fragmentation and branching ratios, are very dependent upon the operating conditions of the instrument. The higher energy of the reagent ions in our system, from alterations to the flow tube voltage and an increase in the flow tube temperature, led to an increase in fragmentation compared to previous studies. Accurate branching ratios are important as, without external calibration, they are used in SIFT-MS measurements in the quantitation of target compounds. Thus ensuring the correct branching ratios and product ions is vital for accurate concentration calculations.

The high tube temperature and ion energies in our system also has a large impact on the humidity dependence of the product ions. We observed no secondary product ions with the H_3O^+ reagent ion under humid conditions. We did however observe primary water clusters with the NO^+ and O_2^+ reagent ions but no secondary or tertiary water clusters. Most of the secondary product ions accounted for little of the overall product ion count, with the largest secondary product ion count still only accounting for 26% of the overall product ion count. The work focusing on varying the conditions described in Section 2.2 and the supplementary information further shows the large impact both flow tube temperature and flow tube voltage have on the production and destruction of humid product ions.

Overall, this study shows that returning SIFT-MS for extra sensitivity has a demonstrable impact on ionisation, which may require reassessment of library records for target compounds. Particularly the addition of a flow tube voltage in the Voice200*ultra* compared to instruments used in previous literature has been shown to cause an increase in fragmentation and an impact on the sensitivity of adduct formation product ions. This study shows the impact of varying the flow tube temperature and flow tube voltage on both the branching ratios and sensitivity of benzene, butanone and butanal. It highlights the importance of ensuring that rate constants and branching ratios used for calibration in SIFT-MS are measured under the same operating conditions as the analyses.

Credit author statement

Ieuan J Roberts: Conceptualization, Methodology, Validation, Formal analysis, Investigation, Writing — original draft, Writing — review & editing, Visualization, Project administration **Lucy J Carpenter**: Conceptualization, Writing — review & editing, Supervision; **Marvin D Shaw**: Conceptualization, Writing — review & editing, Supervision; **Vaughan S Langford**: Writing — review & editing.

Funding sources

Declaration of competing interest

The authors declare that they have no known competing financial interests or personal relationships that could have appeared to influence the work reported in this paper.

Acknowledgements

Appendix A. Supplementary data

Supplementary data to this article can be found online at https://doi.org/10.1016/j.ijms.2022.116892.

References

[1] C. Potter, S. Klooster, D. Bubenheim, H.B. Singh, R. Myneni, Modeling terrestrial biogenic sources of oxygenated organic emissions, Earth Interact. 7 (2003) 1−15.

[2] J. Kesselmeier, M. Staudt, Biogenic volatile organic compounds (VOC): an overview on emission, physiology and ecology, J. Atmos. Chem. 33 (1999) 23−88.

[3] X.-F. Huang, et al., Sources of oxygenated volatile organic compounds (OVOCs) in urban atmospheres in North and South China, Environ. Pollut. 261 (2020) 114152−114159.

[4] P. Gu, T.R. Dallmann, H.Z. Li, Y. Tan, A.A. Presto, Quantifying Urban spatial variations of anthropogenic VOC concentrations and source contributions with a mobile sampling platform, Int. J. Environ. Res. Publ. Health 16 (2019) 1632−1652.

[5] J. Calvert, A. Mellouki, J. Orlando, M. Pilling, T. Wallington, Mechanisms of Atmospheric Oxidation of the Oxygenates, Oxford University Press, 2011, https://doi.org/10.1093/oso/9780199767076.001.0001.

[6] G.S. Tyndall, et al., Atmospheric chemistry of small organic peroxy radicals, J. Geophys. Res. Atmos. 106 (2001) 12157−12182.

[7] F. Vichi, et al., Air pollution survey across the western Mediterranean Sea: overview on oxygenated volatile hydrocarbons (OVOCs) and other gaseous pollutants, Environ. Sci. Pollut. Res. 26 (2019) 16781−16799.

[8] A. Mellouki, T.J. Wallington, J. Chen, Atmospheric chemistry of oxygenated volatile organic compounds: impacts on air quality and climate, Chem. Rev. 115 (2015) 3984−4014.

[9] S.-Y. Xia, et al., Long-term observations of oxygenated volatile organic compounds (OVOCs) in an urban atmosphere in southern China, 2014−2019, Environ. Pollut. 270 (2021) 116301−116312.

[10] Z. Du, J. Mo, Y. Zhang, Risk assessment of population inhalation exposure to volatile organic compounds and carbonyls in urban China, Eviron. Int. 73 (2014) 33−45.

[11] A.C. Lewis, et al., Sources and sinks of acetone, methanol, and acetaldehyde in North Atlantic marine air, Atmos. Chem. Phys. 5 (2005) 1963−1974.

[12] X. Tie, A. Guenther, E. Holland, Biogenic methanol and its impacts on tropospheric oxidants, Geophys. Res. Lett. 30 (ASC 3-1-ASC) (2003) 3−4.

[13] L.K. Whalley, et al., The chemistry of OH and HO_2 radicals in the boundary layer over the tropical Atlantic Ocean, Atmos. Chem. Phys. 10 (2010) 1555−1576.

[14] J.-F. Müller, G. Brasseur, Sources of upper tropospheric HO X : a three-dimensional study, J. Geophys. Res. Atmos. 104 (1999) 1705−1715.

[15] I. Folkins, R. Chatfield, Impact of acetone on ozone production and OH in the upper troposphere at high NO x, J. Geophys. Res. Atmos. 105 (2000) 11585−11599.

[16] J. Kirkby, et al., Ion-induced nucleation of pure biogenic particles, Nature 533 (2016) 521−526.

[17] J. Tröstl, et al., The role of low-volatility organic compounds in initial particle growth in the atmosphere, Nature 533 (2016) 527−531.

[18] X. Zhou, K. Mopper, Carbonyl compounds in the lower marine troposphere over the Caribbean Sea and Bahamas, J. Geophys. Res. Oceans 98 (1993) 2385−2392.

[19] X. Zhou, K. Mopper, Apparent partition coefficients of 15 carbonyl compounds between air and seawater and between air and freshwater; implications for air-sea exchange, Environ. Sci. Technol. 24 (1990) 1864−1869.

[20] R.L. Tanner, B. Zielinska, E. Uberna, G. Harshfield, A.P. McNichol, Concentrations of carbonyl compounds and the carbon isotopy of formaldehyde at a coastal site in Nova Scotia during the NARE summer intensive, J. Geophys. Res. Atmos. 101 (1996) 28961−28970.

[21] P.B. Shepson, et al., Sources and sinks of carbonyl compounds in the Arctic Ocean boundary layer: polar ice floe experiment, J. Geophys. Res. Atmos. 101 (1996) 21081−21089.

[22] H. Singh, et al., Evidence from the Pacific troposphere for large global sources of oxygenated organic compounds, Nature 410 (2001) 1078−1081.

[23] J. Lelieveld, et al., Global air pollution crossroads over the Mediterranean, Science 298 (2002) 794–799.

[24] S.S.H. Ho, et al., Biases in ketone measurements using DNPH-coated solid sorbent cartridges, Anal. Methods 6 (2014) 967–974.

[25] P. Romagnoli, et al., Air quality study in the coastal city of Crotone (Southern Italy) hosting a small-size harbor, Environ. Sci. Pollut. Res. Int. 24 (2017) 25260–25275.

[26] V. Michoud, et al., Organic carbon at a remote site of the western Mediterranean Basin: sources and chemistry during the ChArMEx SOP2 field experiment, Atmos. Chem. Phys. 17 (2017) 8837–8865.

[27] K.H. Lui, et al., Seasonal behavior of carbonyls and source characterization of formaldehyde (HCHO) in ambient air, Atmos. Environ. 152 (2017) 51–60.

[28] J.W. Bottenheim, et al., Depletion of lower tropospheric ozone during arctic spring: the polar sunrise experiment 1988, J. Geophys. Res. Atmos. 95 (1990) 18555–18568.

[29] A. Wisthaler, A. Hansel, R. Dickerson, P. Crutzen, Organic trace gas measurements by PTR-MS during INDOEX 1999, J. Geophys. Res. Atmos. 107 (2002) INX2 23-1–INX2 23-11, https://doi.org/10.1029/2001JD000576.

[30] H.B. Singh, et al., Oxygenated volatile organic chemicals in the oceans: inferences and implications based on atmospheric observations and air-sea exchange models, Geophys. Res. Lett. 30 (ASC 13-1-ASC) (2003) 13–15.

[31] K.A. Read, et al., Multiannual observations of acetone, methanol, and acetaldehyde in remote tropical Atlantic air: implications for atmospheric OVOC budgets and oxidative capacity, Environ. Sci. Technol. 46 (2012) 11028–11039.

[32] B. Derstroff, et al., Volatile organic compounds (VOCs) in photochemically aged air from the eastern and western Mediterranean, Atmos. Chem. Phys. 17 (2017) 9547–9566.

[33] S. Solberg, C. Dye, N. Schmidbauer, A. Herzog, R. Gehrig, Carbonyls and non-methane hydrocarbons at rural European sites from the mediterranean to the arctic, J. Atmos. Chem. 25 (1996) 33–66.

[34] J. Williams, et al., Measurements of organic species in air and seawater from the tropical Atlantic, Geophys. Res. Lett. 31 (2004) L23S06.

[35] C. Marandino, W. Bruyn, S. Miller, M. Prather, E. Saltzman, Oceanic uptake and the global atmospheric acetone budget, Geophys. Res. Lett. 32 (2005), L15806.

[36] S. Wang, et al., Atmospheric acetaldehyde: importance of air-sea exchange and a missing source in the remote troposphere, Geophys. Res. Lett. 46 (2019) 5601–5613.

[37] S.J. Lawson, et al., Seasonal in situ observations of glyoxal and methylglyoxal over the temperate oceans of the Southern Hemisphere, Atmos. Chem. Phys. 15 (2015) 223–240.

[38] K.H. Bates, et al., The global budget of atmospheric methanol: new constraints on secondary, oceanic, and terrestrial sources, J. Geophys. Res. Atmos. 126 (2021), e2020JD033439.

[39] A.B. Thames, et al., Missing OH reactivity in the global marine boundary layer, Atmos. Chem. Phys. 20 (2020) 4013–4029.

[40] X. Zhou, K. Mopper, Photochemical production of low-molecular-weight carbonyl compounds in seawater and surface microlayer and their air-sea exchange, Mar. Chem. 56 (1997) 201–213.

[41] S. Zhou, et al., Formation of gas-phase carbonyls from heterogeneous oxidation of polyunsaturated fatty acids at the air-water interface and of the sea surface microlayer, Atmos. Chem. Phys. 14 (2014) 1371–1384.

[42] E.L. Mungall, et al., Microlayer source of oxygenated volatile organic compounds in the summertime marine Arctic boundary layer, Proc. Natl. Acad. Sci. USA 114 (2017) 6203–6208.

[43] R. Ciuraru, et al., Unravelling new processes at interfaces: photochemical isoprene production at The sea surface, Environ. Sci. Technol. 49 (2015) 13199–13205.

[44] S. Rossignol, et al., Atmospheric photochemistry at a fatty acid–coated air-water interface, Science 353 (2016) 699–702.

[45] L. Tinel, et al., Mechanistic insights on the photosensitized chemistry of a fatty acid at the air/water interface, Environ. Sci. Technol. 50 (2016) 11041–11048.

[46] O. Vesna, M. Sax, M. Kalberer, A. Gaschen, M. Ammann, Product study of oleic acid ozonolysis as function of humidity, Atmos. Environ. 43 (2009) 3662–3669.

[47] A.K.Y. Lee, C.K. Chan, Heterogeneous reactions of Linoleic acid and Linolenic acid particles with ozone: reaction pathways and changes in particle mass, Hygroscopicity, and Morphology, J. Phys. Chem. A 111 (2007) 6285–6295.

[48] J. Zahardis, G.A. Petrucci, The oleic acid-ozone heterogeneous reaction system: products, kinetics, secondary chemistry, and atmospheric implications of a model system – a review, Atmos. Chem. Phys. 7 (2007) 1237–1274.

[49] B.J. Prince, D.B. Milligan, M.J. McEwan, Application of selected ion flow tube mass spectrometry to real-time atmospheric monitoring, Rapid Commun. Mass Spectrom. 24 (2010) 1763–1769.

[50] R.L. Wagner, et al., Application of a mobile laboratory using a selected-ion flow-tube mass spectrometer (SIFT-MS) for characterisation of volatile organic compounds and atmospheric trace gases, Atmos. Meas. Tech. 14 (2021) 6083–6100.

[51] T.T. Hien, et al., Comprehensive volatile organic compound measurements and their implications for ground-level ozone formation in the two main urban areas of Vietnam, Atmos. Environ. 269 (2022), 118872.

[52] D. Smith, P. Španěl, Selected ion flow tube mass spectrometry (SIFT-MS) for on-line trace gas analysis, Mass Spectrom. Rev. 24 (2005) 661–700.

[53] P. Španěl, Y. Ji, D. Smith, SIFT studies of the reactions of H3O+, NO+ and O2+ with a series of aldehydes and ketones, Int. J. Mass Spectrom. Ion Process. 165–166 (1997) 25–37.

[54] P. Španěl, D. Smith, SIFT studies of the reactions of H3O+, NO+ and O2+ with a series of alcohols, Int. J. Mass Spectrom. Ion Process. 167–168 (1997) 375–388.

[55] P. Španěl, J. Žabka, I. Zymak, D. Smith, Selected ion flow tube study of the reactions of H3O+ and NO+ with a series of primary alcohols in the presence of water vapour in support of selected ion flow tube mass spectrometry, Rapid Commun. Mass Spectrom. 31 (2017) 437–446.

[56] C. Bettenhausen, K. Podcast Jansen, How Did We Get to Helium Shortage 4.0? Chemical & Engineering News, 2022.

[57] D. Kramer, Helium is again in short supply, Phys. Today (2022), https://doi.org/10.1063/PT.6.2.20220404a.

[58] D. Smith, M.J. McEwan, P. Španěl, Understanding gas phase ion chemistry is the key to reliable selected ion flow tube-mass spectrometry analyses, Anal. Chem. 92 (2020) 12750–12762.

[59] M. Ghislain, et al., Direct analysis of aldehydes and carboxylic acids in the gas phase by negative ionization selected ion flow tube mass spectrometry: quantification and modelling of ion–molecule reactions, Rapid Commun. Mass Spectrom. 33 (2019) 1623–1634.

[60] R.D. Cates, M.T. Bowers, Energy transfer in ion-molecule association reactions. Dependence of collisional stabilization efficiency on the collision gas, J. Am. Chem. Soc. 102 (1980) 3994–3996.

[61] P. Španěl, D. Smith, Selected ion flow tube studies of the reactions of H3O+, NO+, and O2+ with several aromatic and aliphatic hydrocarbons, Int. J. Mass Spectrom. 181 (1998) 1–10.

[62] P. Španěl, M. Pavlik, D. Smith, Reactions of H3O+ and OH− ions with some organic molecules; applications to trace gas analysis in air, Int. J. Mass Spectrom. Ion Process. 145 (1995) 177–186.

[63] P. Španěl, J.M.V. Doren, D. Smith, A selected ion flow tube study of the reactions of H3O+, NO+, and O2+ with saturated and unsaturated aldehydes and subsequent hydration of the product ions, Int. J. Mass Spectrom. 213 (2002) 163–176.

[64] D. Smith, T. Wang, P. Španěl, Analysis of ketones by selected ion flow tube mass spectrometry, Rapid Commun. Mass Spectrom. 17 (2003) 2655–2660.

[65] G.D.A. Mitchell, Review of permeation tubes and permeators, Separ. Purif. Methods 29 (2000) 119–128.

[66] B.E. Saltzman, W.R. Burg, G. Ramaswamy, Performance of permeation tubes as standard gas sources, Environ. Sci. Technol. 5 (1971) 1121–1128.

[67] C. Schlundt, et al., Oxygenated volatile organic carbon in the western Pacific convective center: ocean cycling, air–sea gas exchange and atmospheric transport, Atmos. Chem. Phys. 17 (2017) 10837–10854.

[68] M. Yang, et al., Air–sea fluxes of oxygenated volatile organic compounds across the Atlantic Ocean, Atmos. Chem. Phys. 14 (2014) 7499–7517.

[69] F. Vichi, et al., Air quality assessment in the central mediterranean sea (Tyrrhenian sea): anthropic impact and miscellaneous natural sources, including volcanic contribution, on the budget of volatile organic compounds (VOCs), Atmosphere 12 (2021) 1609.

[70] N. Wang, et al., Measurements of carbonyl compounds around the Arabian Peninsula: overview and model comparison, Atmos. Chem. Phys. 20 (2020) 10807–10829.

[71] L.G. Huey, Measurement of trace atmospheric species by chemical ionization mass spectrometry: speciation of reactive nitrogen and future directions, Mass Spectrom. Rev. 26 (2007) 166–184.

[72] W. Lindinger, A. Hansel, A. Jordan, On-line monitoring of volatile organic compounds at pptv levels by means of proton-transfer-reaction mass spectrometry (PTR-MS) medical applications, food control and environmental research, Int. J. Mass Spectrom. Ion Process. 173 (1998) 191–241.

[73] K. Sekimoto, et al., Calculation of the sensitivity of proton-transfer-reaction mass spectrometry (PTR-MS) for organic trace gases using molecular properties, Int. J. Mass Spectrom. 421 (2017) 71–94.

[74] D. Smith, T.W.E. Chippendale, P. Španěl, Reactions of the selected ion flow tube mass spectrometry reagent ions H3O+ and NO+ with a series of volatile aldehydes of biogenic significance, Rapid Commun. Mass Spectrom. 28 (2014) 1917–1928.

[75] C. Warneke, C. van der Veen, S. Luxembourg, J.A. de Gouw, A. Kok, Measurements of benzene and toluene in ambient air using proton-transfer-reaction mass spectrometry: calibration, humidity dependence, and field intercomparison, Int. J. Mass Spectrom. 207 (2001) 167–182.